

Skin cancer diagnosis using NIR spectroscopy data of skin lesions *in vivo* using machine learning algorithms

Flavio P. Loss^{a,h}, Pedro H. da Cunha^{d,h}, Matheus B. Rocha^{a,b,h}, Madson Poltronieri Zanoni^{c,h}, Leandro M. de Lima^{a,b,h}, Isadora Tavares Nascimento^f, Isabella Rezende^f, Tania R. P. Canuto^{f,i}, Luciana de Paula Vieira^{f,i}, Renan Rossoni^{f,i}, Maria C. S. Santos^{g,h}, Patricia Lyra Frasson^{e,f,h}, Wanderson Romão^{d,h,j}, Paulo R. Filgueiras^{d,h}, Renato A. Krohling^{a,b,h}

^a*Labcin - Nature Inspired Computing Lab.*

^b*PPGI - Graduate Program in Computer Science*

^c*Department of Chemistry*

^d*PPGQ - Graduate Program in Chemistry*

^e*Department of Specialized Medicine*

^f*Dermatological Assistance Program (PAD)*

^g*Pathological Anatomy Unit of the University Hospital Cassiano Antônio Moraes (HUCAM)*

^h*Federal University of Espírito Santo (UFES), Vitória, ES, 29075-910, Brazil*

ⁱ*Secretary of Health of the Espírito Santo State, Vitória, Brazil*

^j*Federal Institute of Espírito Santo (IFES), Vitória, ES, 29040-780, Brazil*

Abstract

Skin lesions are classified in benign or malignant. Among the malignant, melanoma is a very aggressive cancer and the major cause of deaths. So, early diagnosis of skin cancer is very desired. In the last few years, there is a growing interest in computer aided diagnostic (CAD) using most image and clinical data of the lesion. Although we have seen an increasing progress in CAD of skin lesions, these sources of information present limitations due to their inability to provide information of the molecular structure of the lesion. NIR spectroscopy may provide an alternative source of information to automated CAD of skin lesions. The most commonly used techniques and classification algorithms used in spectroscopy are Principal Component Analysis (PCA), Partial Least Squares - Discriminant Analysis (PLS-DA),

Email address: krohling.renato@gmail.com corresponding author (Renato A. Krohling)

and Support Vector Machines (SVM). Nonetheless, there is a growing interest in applying the modern techniques of machine and deep learning (MDL) to spectroscopy. One of the main limitations to apply MDL to spectroscopy is the lack of public datasets. Since there is no public dataset of NIR spectral data to skin lesions, as far as we know, an effort has been made and a new dataset named NIR-SC-UFES, has been collected, annotated and analyzed generating the gold-standard for classification of NIR spectral data to skin cancer. Next, the machine learning algorithms XGBoost, CatBoost, LightGBM, 1D-convolutional neural network (1D-CNN) and standard algorithms as SVM and PLS-DA were investigated to classify cancer and non-cancer skin lesions. Experimental results indicate the best performance obtained by LightGBM with pre-processing using standard normal variate (SNV), feature extraction and data augmentation with Generative Adversarial Networks (GAN) providing values of 0.839 for balanced accuracy, 0.851 for recall, 0.852 for precision, and 0.850 for F-score. The obtained results indicate the first steps in CAD of skin lesions aiming the automated triage of patients with skin lesions *in vivo* using NIR spectral data.

Keywords: machine learning, 1D-convolutional neural network, skin cancer, Near-Infrared (NIR) spectroscopy, dataset of skin lesions collected *in vivo*

1. Introduction

In recent years, machine and deep learning algorithms have provided promising results in several areas of knowledge that were previously dominated by statistical or mathematical approaches, indicating also potential to spectral data (Ramirez et al., 2021). However, machine learning algorithms, and especially deep learning algorithms, need a significant amount of data to perform well (Ng et al., 2020).

One of the first works reporting the application of spectroscopy in the detection of skin cancer is due to McIntosh et al. (2002). They used Linear Discriminant Analysis (LDA) to classify skin lesions with promising results. Next, Gniadecka et al. (2004) used artificial neural networks to classify spectral data skin lesions obtaining satisfactory results.

Convolutional Neural Networks (CNN) have also been applied to achieve better spectral data classification results, mainly due to the pre-processing and feature extraction capability provided by the convolutional layers (Liu et al., 2017; Malek et al., 2017). Morais et al. (2020) and Zeng et al. (2021)

tackle the spectral data classification problem with the K-Nearest Neighbors (KNN) algorithm.

Data related to infrared spectroscopy of skin lesions present characteristics such as the presence of high-dimensional data, class imbalance and low number of samples, requiring yet additional research efforts to ensure better classification performance.

Araújo et al. (2021) presents an algorithm for extracting pre-established statistical features of Raman spectral data of skin lesions and they applied the Light Gradient Boosting Machine (LightGBM) (Ke et al., 2017) as a classification algorithm with promising results to discriminate between nevus and melanoma.

Several advanced gradient boosting machine (GBM) algorithms have been proposed in recent years, such as, the eXtreme Gradient Boosting (XGBoost) (Chen and Guestrin, 2016), Categorical Boosting (CatBoost) (Prokhorenkova et al., 2019), and the Light Gradient Boosting Machine (LightGBM). These advanced GBM algorithms have provided state of the art results in classification problems.

This paper aims to investigate the performance of machine and deep learning algorithms for classification of spectral data of the main skin lesions. Since there is no public dataset of NIR spectral data to skin lesions, as far as we know, a new dataset named NIR-SC-UFES, has been collected, annotated and analyzed generating the gold-standard for classification of NIR spectral data to skin cancer. The algorithms XGBoost, CatBoost, LightGBM and 1D-convolutional neural network (1D-CNN) were investigated to classify cancer and non-cancer skin lesions and they are also compared with the standard algorithms PLS-DA and SVM used in chemometrics.

The main contributions of this work are as in the following:

- We provide a new dataset named NIR-SC-UFES of the most common skin lesions not yet available in the literature.
- We perform extensive experiments with the most powerful machine learning algorithms XGBoost, CatBoost, LightGBM and 1D-CNN to classify the NIR spectral dataset.
- We investigate the influence of pre-processing and feature extraction as well data augmentation techniques to tackle small datasets.

The paper is organized as follows: Section 2 describes the data collection process of a new NIR spectral dataset for the most common skin lesions.

In addition, we tackle the data pre-processing, feature extraction and data imbalance between classes. In Section 3, the machine and deep learning algorithms and the method to carry out the experiments are described. In Section 4, the results and discussions are presented. Section 5 ends up with conclusions and directions for future research.

2. Data and Preprocessing

2.1. The NIR-SC-UFES Dataset

By means of a partnership with the Dermatological and Surgical Assistance Program (*in Portuguese: Programa de Assistência Dermatológica e Cirúrgica*, PAD) at the University Hospital Cassiano Antônio Moraes (Hucam) of the Federal University of Espírito Santo (UFES), a dataset of skin lesions was created. The PAD-UFES-20 dataset (Pacheco et al., 2020) is composed of the six most common skin diseases: 1) cancer, which consists of melanoma (MEL), basal cellular carcinoma (BCC) and squamous cellular carcinoma (SCC); and 2) non-cancer, which consists of nevus (NEV), actinic keratosis (ACK) and seborrheic keratosis (SEK).

The PAD-UFES-20 dataset consists of images taken from smartphones and metadata (patient and collected lesion information). Despite the importance of images in automated diagnostics, there are specific lesions such as MEL and NEV that are harder or even impossible to detect cancerous patterns using clinical images or patient lesion information (Pacheco and Krohling, 2020). Studies (Pacheco and Krohling, 2020) were carried out to automatically recognize the main skin lesions. However, there are still difficulties in correctly discriminating all types of skin lesions, especially in differentiating between MEL and NEV and between MEL and both the keratosis (SEK and ACK). Figure 1 shows the most common six skin lesions investigated in this work.

McIntosh et al. (2002) investigated the use of Near-Infrared (NIR) spectroscopy by differentiating some types of skin lesions such as NEV and MEL. Spectroscopy measures the amount of light reflected at such wavelengths, when incident on the molecule to be analyzed, being a non-invasive and fast approach (Stuart, 2004).

In the search for an alternative source of information to detecting skin cancer, a new dataset, named NIR-SC-UFES, was collected using near infrared spectroscopy alongside the PAD program. From March, 2021 to December,

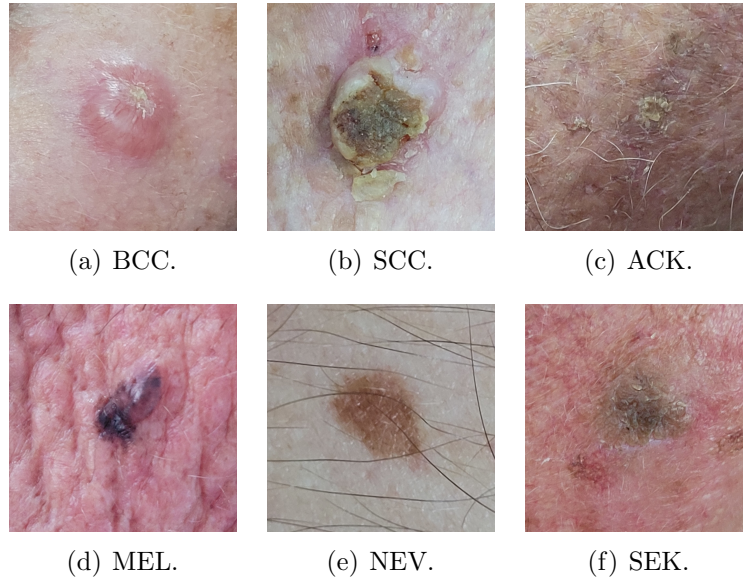


Figure 1: A photo sample of each type of skin lesion investigated in this work.

2022, the collection of the spectral data of skin lesions was carried out using the Micronir spectrometer. The number of dimensions of each sample consists of 125 amplitude values in the wavelength range of 900 nm to 1700 nm, each one representing the average measured in an interval of 6.4 nm. Figure 2 shows the process of data collection using the portable Micronir spectrometer.

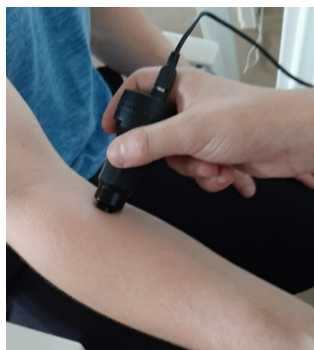


Figure 2: Acquisition of the NIR spectral data of a patient lesion using the Micronir portable spectrometer.

For benign skin lesions the diagnostic is performed by a committee of 3 dermatologists and for malignant skin lesions the result of the biopsy is the gold-standard. For the classification of skin lesions, two different labels will be considered, the non-cancer, which contains spectra of the samples of ACK, SEK and NEV; and cancer referring to the spectra of samples of BCC, SCC and MEL. A well known problem in the skin cancer diagnosis using CAD is the low number of samples and the imbalance between classes. The NIR-SC-UFES dataset contains 586 samples of benign lesions and 385 of malignant, totaling 971 samples. This corresponds to 60.4% of the samples are non-cancer and 39.6% are cancer. Counting each lesion specifically, the dataset contains 336 ACK samples, 188 SEK, 62 NEV, 302 BCC, 72 SCC and 11 MEL.

Figure 3 shows a spectral data sample of the six kind of skin lesions contained in the NIR-SC-UFES dataset.

In the field of chemometrics, it is commonly used traditional algorithms to work with spectral data, such as *Partial Least Squares* (PLS) (Brereton, 2015). However, the use of machine learning and deep learning algorithms are increasingly used for this type of task, providing superior results to those obtained by standard algorithms of chemometrics (Yuanyuan and Zhibin, 2018). Some of these models may face greater difficulty in generalizing with a reduced amount of training data, due to their architecture and training method. In this paper, we apply the most powerful machine learning algorithms XGBoost, CatBoost, LightGBM and 1D convolutional neural networks to the NIR-SC-UFES dataset to classify skin cancer. In addition, we investigate the effects of pre-processing and data augmentation methods in

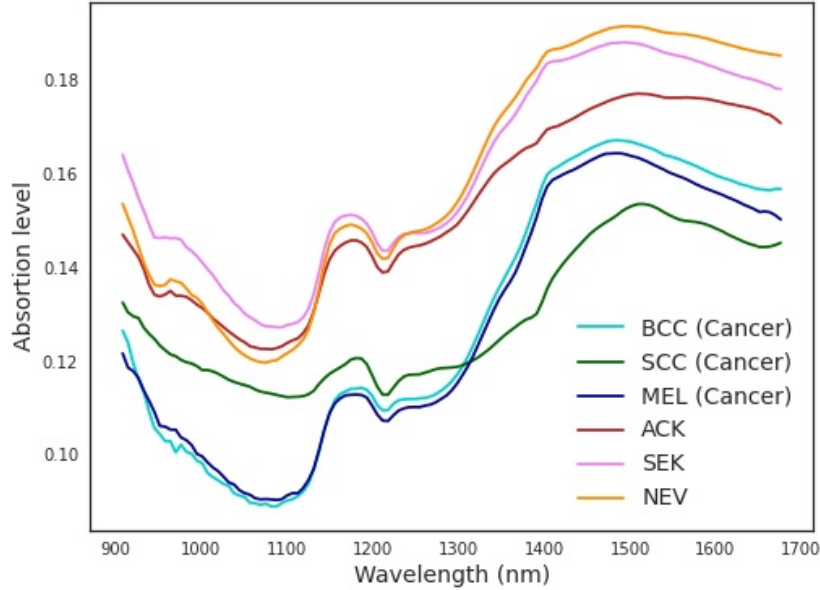


Figure 3: Spectral data sample of the six kind of skin lesions contained in the NIR-SC-UFES dataset.

the performance of the algorithms.

2.2. Pre-processing

Data coming from a spectrometer are susceptible to various types of noise, whether due to external interference or the precision of the equipment (Smulko et al., 2015). So, data pre-processing techniques are applied to the spectral data. The dispersion of the radiation is dependent on the physical nature of the sample particles. For the correction of such divergences, techniques of centralization of each individual sample are used, being the *Standard Normal Variate* (SNV) highly used for the removal of such components (Barnes et al., 1989).

The SNV value is calculated by:

$$SNV = (y_i - \bar{y}) / \sqrt{\sum_{i=1}^n (y_i - \bar{y})^2 / (n - 1)}$$

where n is the number of wavelengths in the sample, y_i is the value of the absorbance at each wavelength i for each sample and \bar{y} is the average of the amplitudes of the wavelengths.

2.3. Feature Extraction

Araújo et al. (2021) presented a feature extraction method for Raman spectral data of skin lesions that provide superior results compared to experiments without feature extraction. The method consists of calculating statistical features in a subsequence of the original signal of the sample. Some parameters need to be defined, such as the subsequence size and the percentage of overlapping between subsequences. The subsequence generated features that were used in this work are listed in Table 1, where $S_{i,m}$ represents a subsequence of the signal, with i the starting point of the substring and m its length.

In order to find the optimal number of subsequences, we optimize the hyper-parameters using TPE (Tree-structured Parzen Estimator) (Bergstra et al., 2011) as sampler. The optimization algorithm was used along with the framework Optuna (Akiba et al., 2019), optimizing for 200 epochs each validation set. The goal is to automatically find out the number of windows and what features generate the best results (for instance, the highest accuracy or recall). For the number of windows, a minimal value of 5 and maximum of 50 was pre-specified.

Feature	Description	Formula
Mean	Simple average of the subsequence.	$\mu_{i,m} = \frac{1}{m} \sum_{k=0}^{m-1} S_{i+k_r}$
Median	Value that separates the major and minor half of a sample.	$M_m = S_{\frac{N+1}{2}}$
Standard Deviation	Measures the amount of spreading of the subsequence.	$\sigma_{i,m} = \sqrt{\frac{1}{m} \sum_{k=0}^{m-1} S_{i+k_r} - \mu_{i,m}}$
Kurtosis	Measures the amount of spreading of the subsequence.	$ku_{i,m} = \frac{\frac{1}{m} \sum_{k=0}^{m-1} (S_{i+k_r} - \mu_{i,m})^4}{(\sigma_{i,m})^4}$
Skewness	Measures the lack of symmetry in the distribution of subsequence values.	$sk_{i,m} = \frac{\frac{1}{m} \sum_{k=0}^{m-1} (S_{i+k_r} - \mu_{i,m})^3}{(\sigma_{i,m})^3}$
Maximum	Maximum value of the subsequence.	$Max_{i,m} = \max(S_{i,m})$
Minimum	Minimum value of the subsequence.	$Min_{i,m} = \min(S_{i,m})$
Peak	Measures the peak value of a subsequence.	$P_m = \max(S_i)$
Peak to Peak	Measures the distance from a signal peak to the valley.	$P_k = \max(S_i) - \min(S_i)$
RMS(Root Mean Square)	Measures the square root of the mean square of the set.	$RMS = \sqrt{\frac{1}{m} \sum_{i=1}^m S_i^2}$
Variance	Measurement of statistical dispersion of the signal.	$Var = \frac{\sum_{i=1}^m (S_i - \mu)^2}{m-1}$
Crest Factor	Shows the ratio between the peak values and the actual waveform value.	$CF = \frac{P_m}{RMS}$

Table 1: Formulae to calculate the extracted features for each subsequence $S_{i,m}$ (Araújo et al., 2021).

2.4. Oversampling with SMOTE

Imbalanced data can generate problems such as biased validation metrics, and models with greater preference for a class, since samples of the majority class was more present in the training data. In order to tackle this issue we use oversampling, which aims to generate synthetic samples of the minority class, in order to balance the data. It is worth mentioning that creation of synthetic data is a common practice in spectroscopy (Abayomi-Alli et al., 2020).

The Synthetic Minority Over-sampling Technique (SMOTE), introduced by Chawla et al. (2002), is a method used for balancing imbalanced datasets. In this approach, the first step is to calculate the number of observations that need to be generated to balance the data. Typically, this number is determined in a way that equalizes the size of the minority class with that of the majority class. By applying SMOTE, synthetic samples are created based on the characteristics of the minority class to increase its representation in the dataset. This helps address the class imbalance issue and improves the performance of machine learning models on such datasets. Next, each iteration selects a random observation from the minority class and with it, the K-Nearest Neighbors is applied, where for each of these neighbors a distance metric is calculated. Finally, the difference between the distances of the instances is obtained, and multiplied by a random number in the interval $[0, 1]$, thus obtaining the position in the feature vector of the generated instance. Algorithm 1 lists the pseudo-code for synthetic sample generation using SMOTE.

2.5. GAN-based Data Augmentation

Generative Adversarial Networks (GANs) is a promising data augmentation technique introduced by Goodfellow et al. (2014). GANs consist of two networks that compete with each other, the generator network G and the discriminator network D . The objective of G is to learn how to generate synthetic data $G(Z)$ similar to the real ones from noise Z , thus the synthetic and real data are used as input in D , being responsible for performing the judgment of the data received, informing whether they are true or false. This competition is described by the loss function:

$$\min_G \max_D \mathcal{L}_{GAN}(G, D) = E_x[\log D(x)] + E_Z[\log(1 - D(G(Z)))]$$

which causes the GANs to generate new samples that differ from the original set.

Algorithm 1 Pseudocode for the SMOTE algorithm

Input: Number of minority class samples T ; Amount of SMOTE $N\%$; Number of nearest neighbours k .
 $numattrs$ = Number of attributes
 $Sample$: Original vector of minority class
 $newindex$: Synthetic sample counter, starting from 0
 $Synthetic$: Synthetic data vector

5: **for** $i = 1$ to T **do**
 Calculate the k nearest neighbours to i .
 Save the indexes in $nnarray$.
 while $N \neq 0$ **do**
 Choose a number between 1 and k , call it nn .
10: This step chooses k nearest neighbours i .
 for $attr = 1 \rightarrow numattrs$ **do**
 $dif = Sample[nnarray[nn]][attr] - Sample[i][attr]$
 $gap =$ random number between 0 and 1
 $Synthetic[newindex][attr] = Sample[i][attr] + gap * dif$
15: **end for**
 $newindex ++$
 $N = N - 1$
 end while
end for

Pavlou and Kourkoumelis (2022) proposed a simple GAN scheme to generate synthetic Raman spectra using data from both healthy and osteoporosis bone samples *ex vivo*. Their scheme works as in the following: the generated data by the GAN and real data are normalized and applied Principal Component Analysis (PCA), where ellipses are generated with a certain confidence interval to evaluate the variability of the augmented data set and data that are outside of the ellipse are considered outliers and consequently discarded. Since this scheme is of general purpose it can be applied to augment any one-dimensional biomedical signal. So, this data augmentation technique was also used in our experiments for generating NIR spectral data for skin lesions aiming to increase the number of samples from the minority class (cancer) to the same size as the majority class (non-cancer). The process works in the following way: the raw data of the NIR spectra referring only to the cancer class were used to train the GAN and obtain new synthetic ma-

ligniant spectra from the real ones. Next, the real and generated data were normalized with the SNV technique to perform the variability analysis and discard possible outliers. The confidence interval used for the ellipses was 95%, i.e., the ellipse that is drawn around the two axes (major and minor) is supposed to contain the 95% of the data points. The GAN structure for our case is shown in Figure 4.

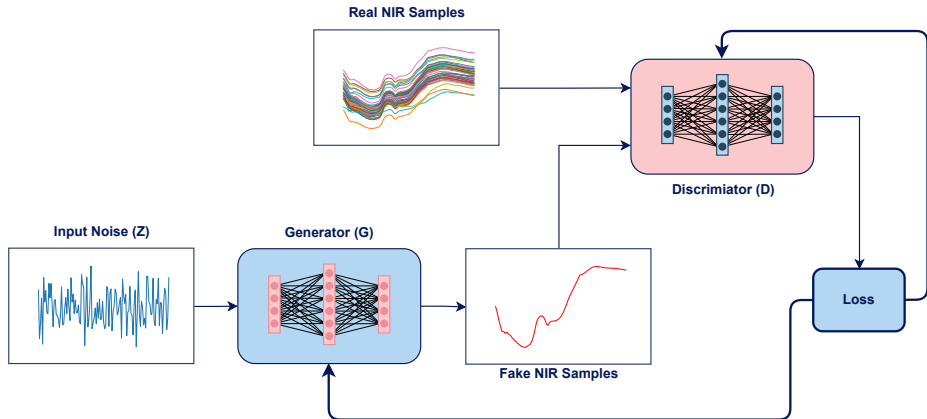


Figure 4: Structure of the GAN network for generating NIR samples. A noise vector Z passes through the generator (G) obtaining the generated output, and the discriminator D is simultaneously trained to distinguish the generated signals from the real ones. The reconstruction loss measures how close the generated signals are to the real ones.

3. Algorithms and Methods

Next, we shortly describe the machine learning algorithms XGBoost, CatBoost, LightGBM, 1D-CNN as well as PLS-DA and SVM used in this work.

3.1. Algorithms

3.1.1. Extreme Gradient Boosting (XGBoost)

The XGBoost algorithm (Chen and Guestrin, 2016) consists of a cast of simple predictors (similar regression trees) also called a weak learner, in which the responses of each individual predictor are aggregated. The set of regression trees that make up the cast is elaborated in two steps: (a) a tree T_0 is built by adding to its structure the branch of the attribute that most improves the predictor at each step and, once its structure is defined, the optimal values are calculated for the l leaves of the tree and (b) the inclusion

of new trees to the set is guided by the residual error of the model, so that new predictors complement the imperfections of the previous ones (Friedman, 2002). Unlike other boosting techniques, Extreme Gradient Boosting is a model that makes use of regularization and overfitting control to improve the performance of the algorithm.

3.1.2. Categorical Boosting (CatBoost)

The CatBoost algorithm (Prokhorenkova et al., 2019) was developed with the purpose of easily handling large datasets as well as heterogeneous data. CatBoost is a combination of the names “category” and “boosting” as it handles categories on its own and is based on the gradient boosting algorithm. CatBoost only requires indexes of categorical features to perform the transformation of categories into numerical data (Hancock et al., 2020), unlike the vast majority of data mining algorithms that require several pre-processing steps. Furthermore, another relevant feature of CatBoost is that it does not require large datasets for training.

3.1.3. Light Gradient Boosting Machine (LightGBM)

The LightGBM algorithm (Ke et al., 2017) was developed to overcome the limitations of the Gradient Boosting Machine (GBM) algorithm in big data problems because the GBM becomes very inefficient due to its construction being carried out according to the number of instances and attributes. Thus, a sampling technique is necessary, i.e., operating with smaller samples to reduce complexity. The LightGBM algorithm implements the sampling technique by the Gradient-Based One-Side Sampling (GOSS) method, since it was observed that different instances of the data present different gradients, and these in turn act in different ways to gain information. Those with greater gradient in absolute values result in greater information gain.

The algorithm seeks to carry out the sampling in order to obtain only instances with the highest gradient, allowing a significant reduction in the data while maintaining a significant part of the information. Another advantage of this sampling is that it allows to reduce noise by keeping only data with high gradients. As a result, the LightGBM algorithm performs faster than traditional GBM algorithms and achieves accuracy equivalent to or greater than those counterparties.

3.1.4. Artificial Neural Networks

A feedforward neural network consists of information processing elements called artificial neurons, which are arranged in layers and are interconnected with each other (Rumelhart et al., 1986). Neural networks are characterized by three types of layers: the input layer, whose neurons receive the primary data directly, the hidden layers that contain the intermediate neurons and perform most of the interconnections between them, and the output layer where, after all the information flows through the network, it assumes the role of the final transformation of the data and represents the output of the network.

Convolutional neural networks differ from feedforward neural networks by having convolution and pooling layers in at least one of its layers, being able to extract spatial and temporal characteristics from data, such as images and time series (Goodfellow et al., 2016). The convolutional layers of one dimension are used due to the unidimensional characteristic of the spectra, and pooling layers to reduce the dimensionality of the output of the convolutional layer (Goodfellow et al., 2016). After feature extraction with the convolution kernels and dimensionality reduction, feedforward networks are used with ReLU activation functions (Nair and Hinton, 2010) and neurons at the output layer with sigmoid activation function. To generate a CNN architecture, convolution and pooling layers were used, followed by a feedforward layer for mapping the relationships between the variables.

3.1.5. Standard Algorithms Used for Spectral Data

Partial Least Squares-Discriminant Analysis (PLS-DA) is a supervised classification method developed based on regression modeling. It is a multivariate dimensionality reduction technique that has been standard in the field of chemometrics over two decades (Gottfries et al., 1995).

Support Vector Machines (SVM) is a supervised learning method and performs well in linear and non-linear modeling due to the kernel mapping that transforms the sample space (Boser et al., 1992). In this study, different types of kernel functions were tested, such as radial basis function, linear and polynomial. For better performance of the SVM, the TPE (Bergstra et al., 2011) was used to optimize three parameters, the cost constant, C , which optimizes the slack variable, the tolerance, ϵ , which delimits the slack, and the gamma constant, γ , which optimizes the kernel function.

3.2. Experimental Methodology

In the following, we describe the experimental methodology to carry out the experiments.

3.2.1. Cross-Validation

Data separation was carried out as follows: from the 971 samples, 776 samples for training (80%) and 195 for testing (20%). This represents a percentage of 60.35%, and 39.65% for non-cancer and cancer samples, respectively. By counting each lesion specifically, the dataset contains 336 ACK, 188 SEK, 62 NEV, 302 BCC, 72 SCC, and 11 MEL samples. The data were stratified according to the amount of injury, ensuring that we have, e.g., 9 MEL (80%) in training and 2 MEL (20%) in testing.

To separate the training data, the Cross-Validation (CV) technique was used. CV is used to avoid methodological errors, it separates the data into k equal parts named folds, with $(k - 1)$ parts used as training data and 1 for validation. This separation is repeated k times, with the validation part at each partition a shift is performed, so that in the end, the entire data set was used in the process. In our experiments, $k = 5$ was used, a default value present in the *sci-kit* library. The CV separates the data between 80% training samples and 20% validation samples into each of the k parts, maintaining stratification based on the skin lesions. Both the separation between training and testing, and that of the CV for training and validation, a seed was used to keep the choice of folders by default for each test. Figure 5 shows a diagram of the dataset split into train and test, and the train dataset split in k folds.

3.2.2. Metrics

To evaluate the performance of the classification algorithms, five common metrics in the literature were used. Accuracy, Balanced Accuracy, Recall, Precision, and F-score respectively, are calculated by:

$$ACC = \frac{TP + TN}{TP + FP + TN + FN} \quad (1)$$

$$BACC = \frac{\frac{TP}{TP+FN} + \frac{TN}{TN+FP}}{2} \quad (2)$$

$$Recall = \frac{TP}{TP + FN} \quad (3)$$

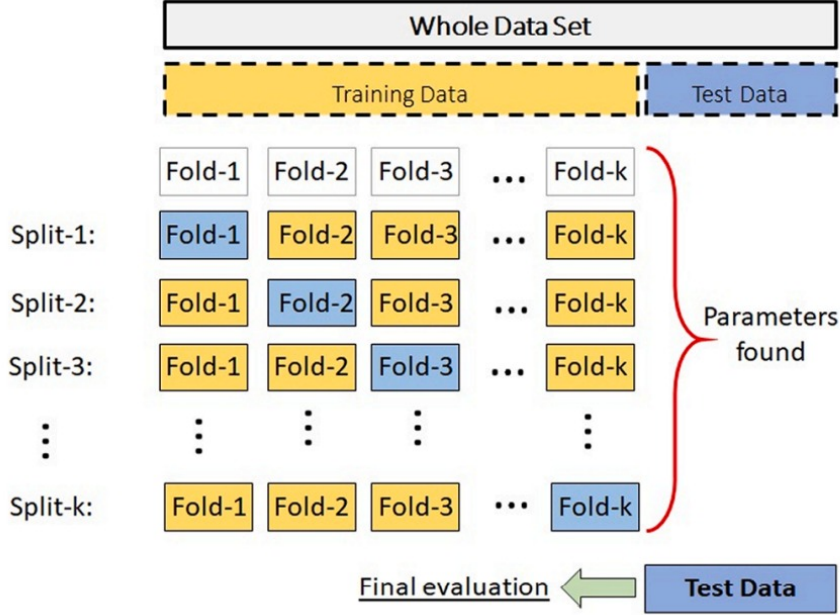


Figure 5: Cross Validation performed using k-fold splits.

$$Precision = \frac{TN}{TN + FP} \quad (4)$$

$$F\text{-score} = 2 * \frac{Recall * Precision}{Recall + Precision} \quad (5)$$

The variables TP , TN , FP , and FN are abbreviations of True Positive, True Negative, False Positive, and False Negative, respectively. For skin lesions classification, it is preferable that the classifier correctly matches the class of cancer lesions, as the patient's condition may be critical and the search for treatment must be immediate.

3.2.3. Hyperparameters setting

Among the algorithms used, XGBoost, CatBoost, LightGBM and 1D-CNN have hyperparameters, which are adjusted to obtain the best performance of the models. The search for optimal hyperparameters was performed using the training set. Next, the best hyperparameter combination was used to train and evaluate the model.

Table 2 presents the hyperparameter search space for XGBoost, CatBoost and LightGBM algorithms.

Algorithm	Hyperparameter	Search space
XGBoost	class weight	[1 ~ 25]
XGBoost	max depth	[1 ~ 15]
XGBoost	number of trees	[10 ~ 100]
XGBoost	learning rate	[0.01 ~ 1]
XGBoost	col sample by tree	[0.5 ~ 1]
XGBoost	subsample	[0.1 ~ 1]
XGBoost	alpha regularization	[0 ~ 20]
XGBoost	lambda regularization	[0 ~ 20]
CatBoost	max depth	[1 ~ 16]
CatBoost	l2 leaf regularization	[1 ~ 40]
CatBoost	number of trees	[1 ~ 200]
CatBoost	colsample by level	[0.1 ~ 1]
CatBoost	learning rate	[0.01 ~ 1]
LightGBM	class weight	[1 ~ 15]
LightGBM	number of trees	[10 ~ 100]
LightGBM	learning rate	[0.01 ~ 1]
LightGBM	leaf number	[20 ~ 5000, step=20]
LightGBM	max depth	[3 ~ 12]

Table 2: Hyperparameter search space for XGBoost, CatBoost and LightGBM algorithms.

For the problem at hand, the 1D-CNN architecture used, consists of up to three layers of convolution and pooling, followed by a fully connected layer. The search space of the hyperparameters of the 1D-CNN network is presented in Table 3.

Algorithm	Hyperparameter	Search space
1D-CNN	learning rate	[0.01, 0.001, 0.0001]
1D-CNN	batch size	[16 ~ 128]
1D-CNN	number of convolutional layers	[1, 2, 3]
1D-CNN	numbers of neurons on convolutional layers	[64 ~ 256]
1D-CNN	numbers of neurons on deep layers	[64 ~ 256]

Table 3: Hyperparameter search space for the 1D-CNN.

4. Experimental Results

In this work we investigate the performance of the machine learning algorithms XGBoost, CatBoost, LightGBM, 1D-CNN as well as the standard algorithms SVM and PLS-DA applied to the new NIR-SC-UFES dataset. In order to address the problem of imbalanced data, two oversampling techniques SMOTE and GAN are used. The experiments are carried out for the 3 sets of data:

- I - Raw spectral data,
- II - Balanced data using SMOTE,
- III - Balanced data using GAN.

For each dataset the experiments are carried out as follows:

- a - Using original spectral data without pre-processing,
- b - Using spectral data pre-processed with SNV,
- c - Using data pre-processed with SNV and with feature extraction.

The results obtained are presented in the following.

4.1. Results obtained using raw data

Table 4 presents the results of the experiments without pre-processing. In bold is highlighted the highest average for each metric and standard deviation.

Algorithm	ACC	BACC	Recall	Precision	F-Score
PLS-DA	0.743 ± 0.004	0.699 ± 0.005	0.494 ± 0.011	0.773 ± 0.005	0.602 ± 0.009
SVM	0.833 ± 0.013	0.809 ± 0.015	0.693 ± 0.033	0.857 ± 0.027	0.766 ± 0.021
XGBoost	0.740 ± 0.017	0.741 ± 0.013	0.748 ± 0.027	0.649 ± 0.029	0.694 ± 0.012
CatBoost	0.771 ± 0.021	0.756 ± 0.023	0.683 ± 0.045	0.724 ± 0.031	0.702 ± 0.029
LightGBM	0.760 ± 0.030	0.757 ± 0.025	0.743 ± 0.015	0.683 ± 0.047	0.711 ± 0.026
1D-CNN	0.805 ± 0.017	0.794 ± 0.007	0.740 ± 0.049	0.768 ± 0.054	0.750 ± 0.007

Table 4: Original raw data without pre-processing.

In this case, SVM provided the best performance in terms of balanced accuracy, followed by 1D-CNN indicating the ability of the convolutional neural network to extract features from the samples.

Algorithm	ACC	BACC	Recall	Precision	F-Score
PLS-DA	0.785 ± 0.006	0.747 ± 0.006	0.566 ± 0.010	0.835 ± 0.016	0.675 ± 0.008
SVM	0.822 ± 0.012	0.795 ± 0.017	0.667 ± 0.042	0.849 ± 0.010	0.746 ± 0.025
XGBoost	0.767 ± 0.025	0.776 ± 0.016	0.818 ± 0.030	0.672 ± 0.044	0.736 ± 0.015
CatBoost	0.791 ± 0.010	0.771 ± 0.014	0.675 ± 0.039	0.768 ± 0.024	0.718 ± 0.020
LightGBM	0.794 ± 0.023	0.788 ± 0.013	0.761 ± 0.081	0.742 ± 0.068	0.744 ± 0.015
1D-CNN	0.805 ± 0.013	0.782 ± 0.018	0.672 ± 0.052	0.805 ± 0.034	0.731 ± 0.025

Table 5: Data pre-processed with SNV.

Table 5 presents the results using SNV. A slight improvement can be noted in all algorithms. This kind of improvement is expected, as SNV is a standard technique for processing spectral data.

Despite the GBM algorithms achieving better results than in the previous experiment, SVM still achieves the best results in all metrics, with a BACC of 0.795.

To finalize the evaluation stage of data pre-processing, Table 6 presents the results using pre-processing with SNV, in addition to the use of feature extraction.

Algorithm	ACC	BACC	Recall	Precision	F-Score
PLS-DA	0.812 ± 0.002	0.778 ± 0.003	0.613 ± 0.010	0.874 ± 0.011	0.721 ± 0.005
SVM	0.791 ± 0.015	0.762 ± 0.014	0.626 ± 0.025	0.803 ± 0.041	0.703 ± 0.019
XGBoost	0.798 ± 0.008	0.802 ± 0.005	0.821 ± 0.025	0.713 ± 0.019	0.762 ± 0.006
CatBoost	0.799 ± 0.010	0.777 ± 0.010	0.672 ± 0.021	0.788 ± 0.022	0.725 ± 0.013
LightGBM	0.820 ± 0.010	0.815 ± 0.004	0.792 ± 0.034	0.764 ± 0.036	0.776 ± 0.004
1D-CNN	-	-	-	-	-

Table 6: Data pre-processed with SNV and feature extraction.

Data processed with feature extraction provided the best results with the

GBM models, especially the LightGBM algorithm with balanced accuracy of 0.815.

The 1D-CNN algorithm was not listed in Table 6, as a manual feature extraction would not make sense as pre-processing since convolution layers act as implicit feature extractors in neural networks.

4.2. Results obtained using SMOTE

For the creation of synthetic samples, only the initial training set was used, generating a balance between the classes, while the validation and test base remains intact.

Algorithm	ACC	BACC	Recall	Precision	F-Score
PLS-DA	0.723 ± 0.007	0.717 ± 0.009	0.685 ± 0.019	0.639 ± 0.007	0.662 ± 0.012
SVM	0.819 ± 0.013	0.812 ± 0.011	0.784 ± 0.021	0.764 ± 0.025	0.773 ± 0.013
XGBoost	0.743 ± 0.020	0.756 ± 0.018	0.818 ± 0.031	0.636 ± 0.024	0.715 ± 0.019
CatBoost	0.757 ± 0.020	0.753 ± 0.020	0.735 ± 0.021	0.678 ± 0.026	0.705 ± 0.022
LightGBM	0.751 ± 0.024	0.754 ± 0.031	0.771 ± 0.085	0.658 ± 0.027	0.708 ± 0.039
1D-CNN	0.774 ± 0.026	0.774 ± 0.023	0.774 ± 0.051	0.695 ± 0.043	0.730 ± 0.026

Table 7: Original data without pre-processing.

Table 7 presents the results using SMOTE without pre-processing. One can notice an improvement in the performance of some models, when compared with data in Table 4. With a greater number of samples, the SVM becomes the best model among those tested with balanced accuracy of 0.812.

Algorithm	ACC	BACC	Recall	Precision	F-Score
PLS-DA	0.743 ± 0.006	0.743 ± 0.007	0.745 ± 0.016	0.652 ± 0.007	0.696 ± 0.009
SVM	0.820 ± 0.008	0.813 ± 0.006	0.779 ± 0.014	0.768 ± 0.021	0.773 ± 0.007
XGBoost	0.778 ± 0.049	0.778 ± 0.035	0.779 ± 0.064	0.711 ± 0.084	0.737 ± 0.032
CatBoost	0.808 ± 0.017	0.795 ± 0.020	0.730 ± 0.047	0.773 ± 0.029	0.750 ± 0.026
LightGBM	0.756 ± 0.030	0.757 ± 0.021	0.763 ± 0.048	0.673 ± 0.049	0.713 ± 0.021
1D-CNN	0.808 ± 0.012	0.788 ± 0.010	0.693 ± 0.031	0.798 ± 0.041	0.741 ± 0.013

Table 8: Data pre-processed with SNV.

Table 8 presents the results using SNV. The model that presented the best balanced accuracy was SVM with value of 0.813.

For the last experiment using SMOTE, Table 9 lists the results using SNV and feature extraction with a value of BACC of 0.790 provided by CatBoost and LightGBM and PLS-DA. The 1D-CNN are not applied in this experiment since convolutional layers extract features of the data implicitly.

Algorithm	ACC	BACC	Recall	Precision	F-Score
PLS-DA	0.798 \pm 0.005	0.790 \pm 0.005	0.753 \pm 0.008	0.740 \pm 0.010	0.747 \pm 0.005
SVM	0.789 \pm 0.013	0.776 \pm 0.016	0.717 \pm 0.041	0.741 \pm 0.019	0.728 \pm 0.021
XGBoost	0.784 \pm 0.011	0.785 \pm 0.009	0.789 \pm 0.027	0.704 \pm 0.023	0.743 \pm 0.010
CatBoost	0.804 \pm 0.019	0.790 \pm 0.018	0.724 \pm 0.025	0.768 \pm 0.034	0.745 \pm 0.022
LightGBM	0.796 \pm 0.009	0.790 \pm 0.010	0.763 \pm 0.025	0.732 \pm 0.016	0.747 \pm 0.012
1D-CNN	-	-	-	-	-

Table 9: Data Pre-processed with SNV, and with feature extraction.

4.3. Results obtained with GAN

Using synthetic samples generated using GAN, table 10 presents the results for the case of no pre-processing is performed.

Algorithm	ACC	BACC	Recall	Precision	F-Score
PLS-DA	0.689 \pm 0.014	0.675 \pm 0.015	0.690 \pm 0.014	0.689 \pm 0.014	0.690 \pm 0.001
SVM	0.818 \pm 0.018	0.787 \pm 0.019	0.818 \pm 0.018	0.827 \pm 0.018	0.812 \pm 0.019
XGBoost	0.771 \pm 0.025	0.762 \pm 0.025	0.771 \pm 0.025	0.772 \pm 0.024	0.771 \pm 0.025
CatBoost	0.788 \pm 0.014	0.769 \pm 0.016	0.788 \pm 0.014	0.787 \pm 0.014	0.785 \pm 0.014
LightGBM	0.787 \pm 0.002	0.779 \pm 0.019	0.788 \pm 0.015	0.788 \pm 0.017	0.788 \pm 0.016
1D-CNN	0.808 \pm 0.014	0.793 \pm 0.018	0.808 \pm 0.014	0.808 \pm 0.014	0.806 \pm 0.014

Table 10: Original spectral data, without pre-processing.

Considering the results of previous experiments with no-preprocessing the data, SVM and 1D-CNN algorithms provide the best results in terms of BACC from original data, while GBM algorithms provided inferior performance in terms of BACC without pre-processing.

Table 11 presents the result using SNV. One observes the performance of SVM in terms of BACC is 0.790. The results indicate in this experiment that SVM provided the best performance for most of the metrics.

Algorithm	ACC	BACC	Recall	Precision	F-Score
PLS-DA	0.712 \pm 0.015	0.699 \pm 0.012	0.712 \pm 0.015	0.712 \pm 0.001	0.712 \pm 0.014
SVM	0.816 \pm 0.014	0.790 \pm 0.019	0.816 \pm 0.014	0.820 \pm 0.013	0.811 \pm 0.016
XGBoost	0.794 \pm 0.030	0.778 \pm 0.038	0.794 \pm 0.030	0.795 \pm 0.031	0.791 \pm 0.033
CatBoost	0.765 \pm 0.009	0.739 \pm 0.012	0.765 \pm 0.009	0.766 \pm 0.010	0.760 \pm 0.010
LightGBM	0.806 \pm 0.023	0.790 \pm 0.024	0.806 \pm 0.023	0.805 \pm 0.024	0.804 \pm 0.023
1D-CNN	0.806 \pm 0.011	0.785 \pm 0.012	0.806 \pm 0.011	0.808 \pm 0.013	0.803 \pm 0.011

Table 11: Data pre-processed with SNV.

Table 12 presents the results for data with SNV and feature extraction. In this experiment, LightGBM presents the best results among all the algorithms with BACC of 0.839. CatBoost also performs very competitive to LightGBM.

Algorithm	ACC	BACC	Recall	Precision	F-Score
PLS-DA	0.771 ± 0.005	0.748 ± 0.006	0.771 ± 0.005	0.770 ± 0.005	0.767 ± 0.006
SVM	0.780 ± 0.033	0.750 ± 0.031	0.780 ± 0.033	0.784 ± 0.036	0.773 ± 0.033
XGBoost	0.798 ± 0.027	0.786 ± 0.023	0.798 ± 0.027	0.804 ± 0.031	0.797 ± 0.025
CatBoost	0.845 ± 0.025	0.819 ± 0.027	0.845 ± 0.025	0.852 ± 0.028	0.840 ± 0.026
LightGBM	0.851 ± 0.017	0.839 ± 0.018	0.851 ± 0.017	0.852 ± 0.017	0.850 ± 0.017
1D-CNN	-	-	-	-	-

Table 12: Data pre-processed with SNV, and with feature extraction.

4.4. Feature Importance with SHAP

We applied the SHAP (SHapley Additive exPlanations) algorithm (Lundberg and Lee, 2017) to assess feature importance of the model and to get a visual representation of the statistical features of the subsequences. The SHAP algorithm can be used to explain the output of any machine learning model. For the skin cancer classification model, it is possible to observe the average absorption value for each subsequence created and see which one is the most relevant to the model. In order to illustrate the SHAP applied to this case, Figure 6 shows the feature importance analysis only for the LightGBM model, which provides the best overall results with SNV, feature extraction and data augmentation with GAN.

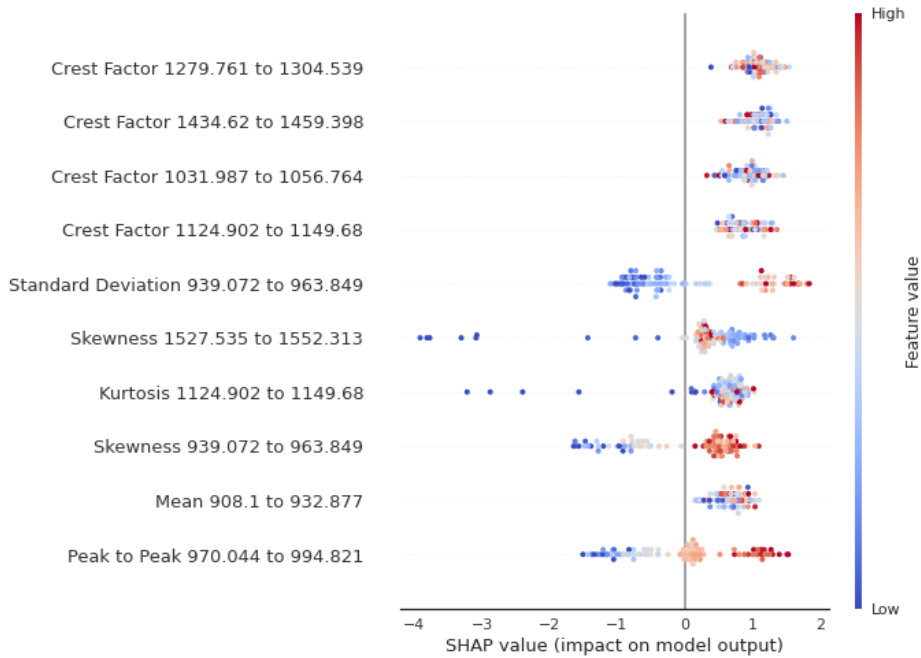


Figure 6: SHAP importance for each feature extracted from the subsequences of the test set. The x axes indicates the calculated SHAP value on the model output, while the y axes display each feature, sorted by its importance for the classifier. The color indicates the original feature value.

The application of SHAP for the LightGBM model provides information that some extracted features such as standard deviation in the wavelength from 939 nm to 963 nm, skewness from 939 nm to 963 nm and peak to peak from 970 nm to 994 nm are important features in the classification.

4.5. Discussion

In terms of overall performance obtained in the experiments, one notes that some algorithms perform better than others depending on the type of pre-processing used. SVM presents consistent performance results in all experiments, while PLS-DA presents slightly worse results without any type of pre-processing, and more competitive ones using extracted features and data augmentation.

GBM algorithms also perform better when feature extraction is used. They achieve the best performance amongst all the experiments using GAN

to generate synthetic samples. In the experiments, Catboost and LightGBM results are very close, with a slightly advantage to LightGBM.

One notices that 1D-CNN present a better performance in reducing false negatives and false positives when the sample signal is pre-processed with SNV. Generally Neural Networks require a large amount of data in its training, which was not the case in this study. Regarding the pre-processing step, convolutional layers work in a way that features are extracted implicitly, and there is no need to extract them. This may represent an advantage of 1D-CNN.

In their work, Araújo et al. (2021) utilized Raman spectra and employed the LightGBM model to obtain the best results. It is worth noting that they worked with a dataset comprising 436 spectral samples, with 168 belonging to nevus and 268 to melanoma. However, the data they utilized for their experiments is not publicly available, thereby making it impossible to directly compare our results.

Krohling et al. (2021) proposed an approach that combines clinical images, clinical information of the lesion, and patients' demographics. They trained a Convolutional Neural Network (CNN) using this aggregated information, achieving an average balanced accuracy of 0.85. Our best-performing LightGBM model investigated in this work using NIR spectral samples reveals a competitive performance in skin cancer detection. It is worth mentioning that our results show promise with the yet limited size of our collected dataset.

Our goal is to publish this dataset as *Data in Brief* and the source code is available under request from authors during submission. After publication, the source code used in our experiments will be available on GitHub.

5. Conclusion

In this paper, we investigate the suitability of NIR spectral data on skin cancer automated diagnosis using machine and deep learning algorithms aiming to develop a triage tool. Firstly, we introduced a new dataset named NIR-SC-UFES composed of spectral samples collected via a portable Micronir spectrometer in the wavelength range of 900 nm to 1700 nm of the most common skin lesions *in vivo* grouped as 1) cancer: melanoma (MEL), basal cellular carcinoma (BCC) and squamous cellular carcinoma (SCC); and 2) non-cancer: nevus (NEV), actinic keratosis (ACK) and seborrheic keratosis (SEK). As far as we know, this is the first time such a dataset is

collected since there is no public dataset available of this sort. Secondly, since the dataset is imbalanced, we use a SMOTE-based data augmentation and GAN-based oversampling to generate synthetic data. Next, we apply the most powerful machine learning algorithms XGBoost, CatBoost, LightGBM, 1D-convolutional neural networks (1D-CNN), as well as standard algorithms as SVM and PLS-DA to our dataset. Experimental results indicate the best performance obtained by LightGBM with pre-processing using standard normal variate (SNV), feature extraction and data augmentation with Generative Adversarial Networks (GAN) providing values of 0.839 for balanced accuracy, 0.851 for recall, 0.852 for precision, and 0.850 for F-score. Through the application of SHAP, we have discovered that the most crucial range of the spectra lies within the interval of 939.072 nm to 994.821 nm. Our dataset NIR-SC-UFES, has a relatively small number of spectral samples for certain skin lesions, particularly melanoma. Indeed, this limitation exists and is currently being addressed. We are exploring additional sources of information to further enhance our results in order to assist doctors in the screening process.

6. Acknowledgments

The authors thank Isadora Tavares Nascimento and Isabella Rezende for the support during the time collecting the dataset NIR-SC-UFES at PAD-UFES. R.A. Krohling thanks the Brazilian research agency Conselho Nacional de Desenvolvimento Científico e Tecnológico (CNPq), Brazil - grant no. 304688/2021-5 and the Fundação de Amparo à Pesquisa e Inovação do Espírito Santo (FAPES), Brazil – grant no. 21/2022. P.F. Filgueiras thanks the support of CNCPq (409700/2022-3, and 305459/2020-1) and Fapes (442/2021, 691/2022 P: 2022-2DRM4, 1036/2022 P: 2022-VZ8G9 e 343/2023 P 2023-6SJK7).

References

- Abayomi-Alli, O.O., Damaševičius, R., Wiczorek, M., Woźniak, M., 2020. Data augmentation using principal component resampling for image recognition by deep learning, in: Artificial Intelligence and Soft Computing: 19th International Conference, ICAISC 2020, Zakopane, Poland, October 12-14, 2020, Proceedings, Part II 19, Springer. pp. 39–48.

- Akiba, T., Sano, S., Yanase, T., Ohta, T., Koyama, M., 2019. Optuna: A next-generation hyperparameter optimization framework, in: Proceedings of the 25th ACM SIGKDD International Conference on Knowledge Discovery & Data Mining, Association for Computing Machinery, New York, NY, USA. p. 2623–2631.
- Araújo, D.C., Veloso, A.A., de Oliveira Filho, R.S., Giraud, M.N., Raniero, L.J., Ferreira, L.M., Bitar, R.A., 2021. Finding reduced Raman spectroscopy fingerprint of skin samples for melanoma diagnosis through machine learning. *Artificial Intelligence in Medicine* 120, 102161.
- Barnes, R.J., Dhanoa, M.S., Lister, S.J., 1989. Standard normal variate transformation and de-trending of near-infrared diffuse reflectance spectra. *Applied Spectroscopy* 43, 772–777.
- Bergstra, J., Bardenet, R., Bengio, Y., Kégl, B., 2011. Algorithms for hyperparameter optimization. *Advances in Neural Information Processing Systems* 24.
- Boser, B.E., Guyon, I.M., Vapnik, V.N., 1992. A training algorithm for optimal margin classifiers, in: Proceedings of the 5th Annual Workshop on Computational Learning Theory, pp. 144–152.
- Brereton, R.G., 2015. Pattern recognition in chemometrics. *Chemometrics and Intelligent Laboratory Systems* 149, 90–96.
- Chawla, N.V., Bowyer, K.W., Hall, L.O., Kegelmeyer, W.P., 2002. SMOTE: Synthetic minority over-sampling technique. *Journal of Artificial Intelligence Research* 16, 321–357.
- Chen, T., Guestrin, C.E., 2016. Xgboost: A scalable tree boosting system. *Knowledge Disc. Data Mining* , 785–794.
- Friedman, J.H., 2002. Stochastic gradient boosting. *Computational Statistics & Data Analysis* 38, 367–378.
- Gniadecka, M., Philipsen, P.A., Wessel, S., Gniadecki, R., Wulf, H.C., Sigurdsson, S., Nielsen, O.F., Christensen, D.H., Hercogova, J., Rossen, K., Thomsen, H.K., Hansen, L.K., 2004. Melanoma diagnosis by Raman spectroscopy and neural networks: Structure alterations in proteins and lipids in intact cancer tissue. *Journal of Investigative Dermatology* 122, 443–449.

- Goodfellow, I., Bengio, Y., Courville, A., 2016. Deep Learning. MIT Press. <http://www.deeplearningbook.org>.
- Goodfellow, I., Pouget-Abadie, J., Mirza, M., Xu, B., Warde-Farley, D., Ozair, S., Courville, A., Bengio, Y., 2014. Generative adversarial nets. *Advances in Neural Information Processing Systems* 27.
- Gottfries, J., K, B., A, W., C., G., 1995. Diagnosis of dementias using partial least squares discriminant analysis. *dementia geriatric cognit disorders. Journal of Big Data* 6(2), 83–8.
- Hancock, T., J., Khosgoftaar, M., T., 2020. Catboost for big data: an interdisciplinary review. *Journal of Big Data* 7, 2196–1115.
- Ke, G., Meng, Q., Finley, T., Wang, T., Chen, W., Ma, W., Ye, Q., Liu, T.Y., 2017. LightGBM: A highly efficient gradient boosting decision tree. *Advances in Neural Information Processing Systems* 30.
- Krohling, B., Castro, P.B., Pacheco, A.G., Krohling, R.A., 2021. A smartphone based application for skin cancer classification using deep learning with clinical images and lesion information. *arXiv preprint arXiv:2104.14353* .
- Liu, J., Osadchy, M., Ashton, L., Foster, M., Solomon, C.J., Gibson, S.J., 2017. Deep convolutional neural networks for Raman spectrum recognition: a unified solution. *The Analyst* 142, 4067–4074.
- Lundberg, S.M., Lee, S.I., 2017. A unified approach to interpreting model predictions. *Advances in Neural Information Processing Systems* 30 (NIP 2017) , 4765–4774.
- Malek, S., Melgani, F., Bazi, Y., 2017. One-dimensional convolutional neural networks for spectroscopic signal regression. *Journal of Chemometrics* 32, e2977.
- McIntosh, L.M., Jackson, M., Mantsch, H.H., Mansfield, J.R., Crowson, A., Toole, J.W., 2002. Near-infrared spectroscopy for dermatological applications. *Vibrational Spectroscopy* 28, 53–58.
- Morais, C.L.M., Lima, K.M.G., Singh, M., Martin, F.L., 2020. Tutorial: multivariate classification for vibrational spectroscopy in biological samples. *Nature Protocols* 15, 2143–2162.

- Nair, V., Hinton, G.E., 2010. Rectified linear units improve restricted Boltzmann machines. *International Conference on Machine Learning*, 807–814.
- Ng, W., Minasny, B., de Sousa Mendes, W., Demattê, J.A.M., 2020. The influence of training sample size on the accuracy of deep learning models for the prediction of soil properties with near-infrared spectroscopy data. *SOIL* 6, 565–578.
- Pacheco, A.G., Krohling, R.A., 2020. The impact of patient clinical information on automated skin cancer detection. *Computers in Biology and Medicine* 116, 103545.
- Pacheco, A.G., Lima, R, G., Salomão, A.S., Krohling, B., Biral, I.P., de Angelo, G.G., Alves Jr, F.C., Esgario, J.G., Simora, C, A., Castro, P.B., et al., 2020. PAD-UFES-20: a skin lesion dataset composed of patient data and clinical images collected from smartphones. *Data in Brief* 32, 106221.
- Pavlou, E., Kourkoumelis, N., 2022. Deep adversarial data augmentation for biomedical spectroscopy: Application to modelling raman spectra of bone. *Chemometrics and Intelligent Laboratory Systems* 228, 104634.
- Prokhorenkova, L., Gusev, G., Vorobev, A., Dorogush, A.V., Gulin, A., 2019. Catboost: unbiased boosting with categorical features. *arXiv:1706.09516*.
- Ramirez, C.A.M., Greenop, M., Ashton, L., ur Rehman, I., 2021. Applications of machine learning in spectroscopy. *Applied Spectroscopy Reviews* 56, 733–763.
- Rumelhart, D.E., Hinton, G.E., Williams, R.J., 1986. Learning representations by back-propagating errors. *Nature* 323, 533–536.
- Smulko, J., Wrobel, M.S., Barman, I., 2015. Noise in biological Raman spectroscopy, in: *International Conference on Noise and Fluctuations (ICNF)*, IEEE. pp. 1–6.
- Stuart, B.H., 2004. *Infrared spectroscopy: fundamentals and applications*. John Wiley & Sons.
- Yuanyuan, C., Zhibin, W., 2018. Quantitative analysis modeling of infrared spectroscopy based on ensemble convolutional neural networks. *Chemometrics and Intelligent Laboratory Systems* 181, 1–10.

Zeng, W., Wang, Q., Xia, Z., Li, Z., Qu, H., 2021. Application of XGBoost algorithm in the detection of SARS-CoV-2 using Raman spectroscopy. *Journal of Physics: Conference Series* 1775, 012007.